ACS APPLIED MATERIALS & INTERFACES

www.acsami.org

Research Article

Deterministic Quantum Light Arrays from Giant Silica-Shelled Quantum Dots

Hao A. Nguyen, David Sharp, Johannes E. Fröch, Yi-Yu Cai, Shenwei Wu, Madison Monahan, Christopher Munley, Arnab Manna, Arka Majumdar, Cherie R. Kagan, and Brandi M. Cossairt*

Cite This: *ACS Appl. Mater. Interfaces* 2023, 15, 4294–4302

Read Online

ACCESS | Metrics & More | Article Recommendations | Supporting Information

ABSTRACT: Colloidal quantum dots (QDs) are promising candidates for single-photon sources with applications in photonic quantum information technologies. Developing practical photonic quantum devices with colloidal materials, however, requires scalable deterministic placement of stable single QD emitters. In this work, we describe a method to exploit QD size to facilitate deterministic positioning of single QDs into large arrays while maintaining their photostability and single-photon emission properties. CdSe/CdS core/shell QDs were encapsulated in silica to both increase their physical size without perturbing their quantum-confined emission and enhance their photostability. These giant QDs were then precisely positioned into ordered arrays using template-assisted self-assembly with a 75% yield for single QDs. We show that the QDs before and after assembly exhibit antibunching behavior at room temperature and their optical properties are retained after an extended period of time. Together, this bottom-up synthetic approach via silica shelling and the robust template-assisted self-assembly offer a unique strategy to produce scalable quantum photonics platforms using colloidal QDs as single-photon emitters.

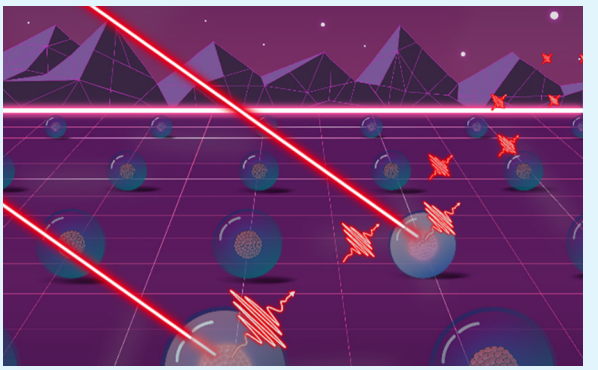

KEYWORDS: *single-photon sources, nanophotonics, quantum dots, silica shelling, deterministic positioning*

1. INTRODUCTION

Quantum nanophotonics holds great potential for several quantum technologies including quantum sensing, quantum computing, and quantum communication.[1,2] However, poor scalability is a critical hurdle that hinders progress in this field. A scalable nanophotonics platform requires replacing traditional bulky table-top optics with chip-scale photonics. One necessary condition for such a scalable platform is the ability to deterministically position single-photon emitters in an array, and subsequent coupling to nanophotonic structures, such as resonators. Although large arrays of nanophotonic cavities have been demonstrated,[3] finding the ideal material for reliable generation of indistinguishable single photons and their scalable integration still remain outstanding challenges.

Among the many material candidates, including self-assembled quantum dots (QDs),[4,5] defects in hexagonal boron nitride,[6−8] diamond,[9,10] two-dimensional materials,[11,12] trapped ions,[13,14] and molecules,[15,16] colloidal QDs have emerged as promising building blocks for integrated photonic systems that provide a unique approach to solve the challenge of deterministic, scalable integration. Colloidal core−shell Cd- and In-based QDs or halide perovskite QDs can be prepared to exhibit strong antibunching behavior, that is, their second-order intensity correlation at zero time delay [$g^{(2)}$ (0)] is less than 0.5 and often approaches zero for a single emitter.[17−23] This makes colloidal QDs competitive candidates for solid-state single-photon sources.

Besides their attractive characteristics for photonic applications including emission wavelength tunability, room temperature stability, and low-cost and flexible synthesis, the key advantage of colloidal QDs is their solution processability. Dispersions of colloidal materials are compatible with various solution-phase integration techniques.[21,22,24,25] Straightforward integration methods, such as spin-coating, drop-casting, capillary assembly, and doctor blade coating, are often performed on patterned or templated substrates with nano- or microscale traps generated by electron beam lithography to enable precise positioning of isolated single QDs.[26−33] Deterministic and scalable positioning of one or a few QDs using these approaches can be realized when the QD size is maximized and/or the size of the predefined trap is minimized.[34,35] A different route for precise placement is to manipulate the location of a QD on a substrate with atomic

Received: October 13, 2022
Accepted: November 28, 2022
Published: December 12, 2022

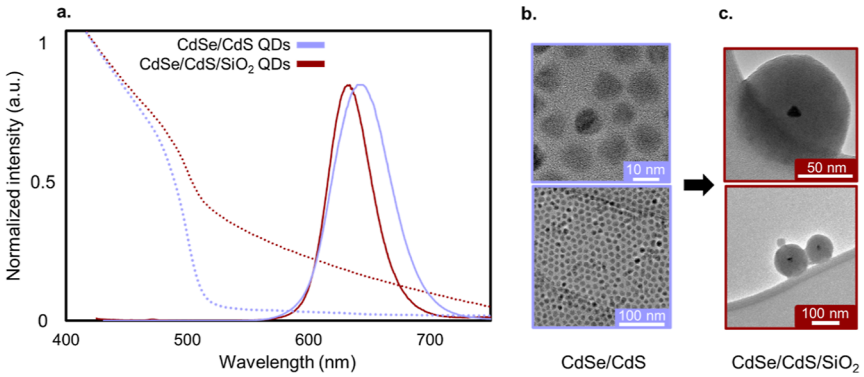

Figure 1. Characterization of the synthesized QDs including (a) photoluminescence (solid curves) and UV−visible absorption spectra (dotted curves), (b) TEM images of CdSe/CdS QDs, and (c) CdSe/CdS/SiO_2 QDs.

force microscopy and/or scanning electron microscopy (SEM) with a nanomanipulator;[36−38] however, this approach does not offer a feasible path to scaling. Most recently, electrohydrodynamic inkjet printing has been demonstrated to deposit droplets of nanoparticles on an array of nanocavities.[39] For this technique, although the production of small ink droplets containing a few nanoparticles was achieved, targeting one particle per droplet remains difficult due to the small size of the nanoparticles and the constraints imposed by the nozzle diameter. Furthermore, implementing available techniques for large-scale patterning of QD single-photon emitters is problematic due to the QD's small size, surface chemistry, and/or poor stability in ambient conditions.[18] Overall, despite intense effort, deterministic positioning of QD single-photon emitters with high scalability remains a challenge.

Here, we demonstrate a bottom-up strategy *via* silica shelling of CdSe/CdS QDs combined with template-assisted self-assembly to deterministically position QD single photon emitters. Applications of silica-shelled QDs are ubiquitous in the biomedical field based on four major advantages: (1) optical transparency, (2) high colloidal, chemical, and optical stability of their dispersions, including in water at different pH values, (3) reduced toxicity of conventional QDs, and (4) versatility of surface modification.[40−45] In this study, we experimentally show that silica shells both increase the physical size of the CdSe/CdS QDs to facilitate device integration and stabilize the QDs to achieve room-temperature single-photon emission. We use the template-assisted self-assembly technique, recently reported for placement of nanoparticles,[46,47] to deterministically deposit single giant silica-shelled CdSe/CdS QDs in ordered arrays wherein they continue to exhibit bright single-photon emission. This synthetic approach provides a scalable and versatile strategy that could be combined with other large-scale placement methods for fabricating quantum nanophotonic devices.

2. RESULTS AND DISCUSSION

2.1. Synthesis and Characterizations of Giant CdSe/CdS/SiO_2 QDs. For core−shell CdSe/CdS QDs, increasing the number of monolayers of the shelling material is a typical approach to achieve larger particle sizes. However, even with the laborious and time-intensive deposition of 19 monolayers of CdS, the QD size only reaches 20 nm in diameter, while a large amount of precursor material is consumed.[48] In addition, an excessively large CdS shell on a CdSe core leads to a reduction in photoluminescence quantum yield (PLQY) due to the formation of interfacial defects caused by lattice strain.[49−51] The optimal PLQY is observed when 8−10 monolayers of CdS are applied to achieve QDs of 10−11 nm in total diameter.[52] Hence, we synthesized wurtzite CdSe/CdS core−shell QDs containing 9 monolayers of CdS with a total diameter of 11 ± 0.4 nm *via* the dual injection method (Figure 1b).[52,53] The synthesized QDs show PL centered around 640 nm with a narrow emission linewidth with a half-width-half-maximum of 27 nm and an 82% PLQY.

To controllably increase the particle size, we encapsulated the CdSe/CdS QDs in silica shells. Synthesis of silica shells on nanoparticles can be achieved usisng two main techniques: the Stöber method and the reverse microemulsion method.[40,54] We used the latter procedure because of its greater degree of control over the particle size and the higher yield for encapsulating one single QD in one silica sphere.[55−57] Generally, the hydrophobic ligands of the initial QDs are replaced by non-ionic surfactant molecules such as IGEPAL CO-520 or Triton X100 in cyclohexane to create a microemulsion. These emulsions act as nanoreactors to control the hydrolysis of the silica precursor, tetraethyl orthosilicate (TEOS), and the resulting silica shell growth using an aqueous ammonia catalyst.

With the reverse microemulsion route, the CdSe/CdS QDs were efficiently encapsulated in silica shells with an average total diameter of 90 ± 18 nm, confirmed by transmission electron microscopy (TEM, Figure 1c). We also observed a small number of hollow silica particles and non-shelled QDs. After the silica shelling process, the PL of the QDs slightly blue-shifted, resulting in a peak maximum at 635 nm with an improved half-width-half-maximum of 20 nm, which are typical behaviors of silanization of QDs (Figure 1a). We also saw an expected drop in PLQY to 34%, which remained the same after 14 months at room temperature as water or ethanol dispersions (Figure S4). This observation indicates that silica shells are effective at protecting QDs from PLQY quenching effects arising from the outside environment. On the other hand, considering the surface ligands and the quasi-type II heterostructure of CdSe/CdS QDs where the electron wavefunction is delocalized over the whole QD and the hole wavefunction is localized in the core, we assume the initial drop in PLQY after the silica shelling process may originate from several aspects including the initial ligand exchange step, the formation of oxidic surface trap sites during the silanization, and lattice strain.[57−59] Several PLQY preservation strategies have been reported including phase-transfer treatment,[41] post-synthetic annealing with UV activation,[60] and QD

https://doi.org/10.1021/acsami.2c18475
ACS Appl. Mater. Interfaces 2023, 15, 4294−4302

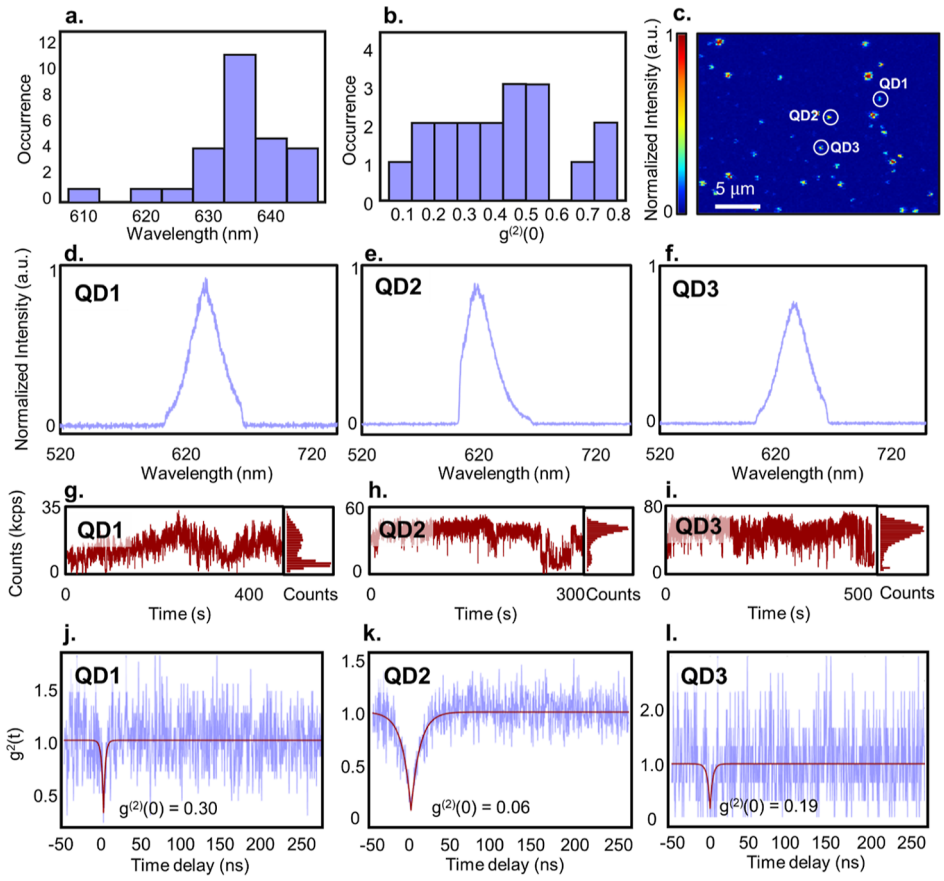

Figure 2. Quantum optical characterization of isolated silica-shelled CdSe/CdS QDs. (a) Distribution of emission maxima of 27 single silica-shelled QDs. (b) Distribution of outcomes from second-order autocorrelation function $g^{(2)}(\tau)$ of 18 single silica-shelled QDs. (c) PL image of single silica-coated QDs on a planar SiO_2 substrate. (d–f) Single particle emission spectra. (g–i) PL intensity time trace. (j–l) Second-order autocorrelation function $g^{(2)}(\tau)$ measurements of three representative single silica-shelled QDs.

core heterostructure engineering,[57,61] which could be used to further improve the final PLQY of the SiO_2-shelled QDs.

3.2. Giant QDs on a Planar Substrate. To test the optical properties of individual giant QDs, we explored spin-coating the colloidal giant QD dispersions on a planar SiO_2 substrate. To avoid aggregation of silica particles caused by interparticle siloxane bonding upon drying, ethanol was used as the solvent. Control over concentration and sonication was also required to achieve either a uniform monolayer or isolated QDs. A small amount (10 μL) of the giant QD stock dispersion in ethanol (100 mg of QDs in 5 mL of ethanol) was directly spin-coated on a planar Si substrate resulting in large clusters of agglomerated nanoparticles. A uniform monolayer of giant QDs was achieved when the same solution was sonicated for 10 min prior to spin-coating. To reach the level of isolated QDs, the original dispersion was diluted by a factor of 100 using ethanol, followed by 10 min of sonication prior to spin-coating (See Section S6 in Supporting Information). To study the single-photon emission of these silica-coated QDs, we performed PL measurements and second-order photon correlation measurements, $g^{(2)}$ (τ). At room temperature and in air, among 46 measured QDs, 19 QDs bleached rapidly, 7 QDs bleached after 4 min, and 20 QDs bleached after 6 min upon continuous wave laser irradiation (532 nm, ~3 μW, ~1 kW cm^{-2}). As photobleaching is assumed to originate from photo–chemical reactions on the surface of the QDs under excitation,[62−65] we initially expected that thick silica shells would reduce this unwanted behavior. However, the photobleaching timescales of the silica-shelled QDs are similar to those of single CdSe-based core/shell QDs.[31,34] Therefore, we hypothesize that the photobleaching phenomenon arises from oxides at the silica–CdS interface, which could be mitigated by applying an insulating layer between the CdS and the silica shells.[62] Figure 2a shows the distribution of the PL maxima of the measured QDs, with most of the emission peaks centered around 635 nm, consistent with PL results from the ensemble dispersion. The PL intensity time trace measurements showed that 15 QDs had a largely unimodal ON state of emission indicating a low blinking behavior. We measured $g^{(2)}(\tau)$ for 18 QDs and found that the $g^{(2)}(0)$ value ranged from 0.06 to 0.79 (Figure 2b). Among them, 12 QDs had $g^{(2)}(0)$ below a threshold of 0.5, with the lowest value of 0.06. Figure 2c–l displays the outcome of single-particle measurements of three representative QDs. Spectral cutoffs at ~600 and 645 nm appear because a bandpass filter was used to reduce background from non-QD emission. Characterization details for other QDs can be found in Sections S8 and S9 in the Supporting Information. These results from isolated silica-shelled QDs including variations in optical behaviors, blinking, photobleaching, and antibunching are analogous to those of isolated Cd-based core/shell QDs in previous studies.[21,23,31,34,66−68]

2.3. Deterministic Positioning of Giant QDs into Arrays. To deterministically position the giant silica-coated QDs into arrays, we employed a template-assisted self-assembly technique that has been demonstrated to precisely

https://doi.org/10.1021/acsami.2c18475
ACS Appl. Mater. Interfaces 2023, 15, 4294−4302

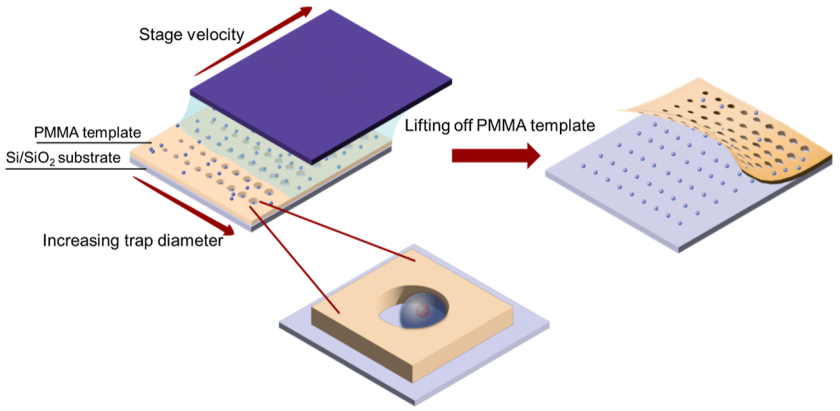

Figure 3. Schematic process of the template-assisted self-assembly method to deterministically place silica (light blue sphere)-shelled QDs (red sphere) in an array using a PMMA template (yellow) on a Si/SiO_2 substrate (light blue).

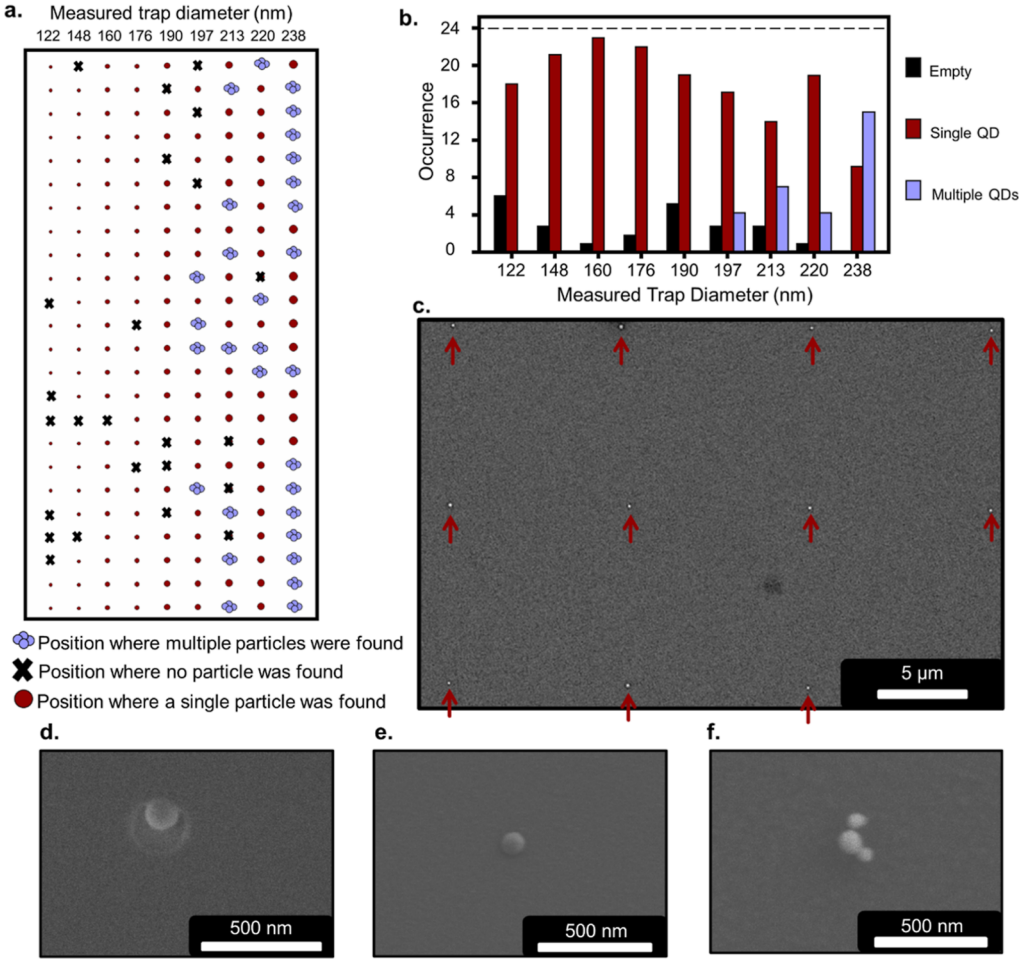

Figure 4. (a) Schematic construction of one 9 × 24 array showing the assembly yield. (b) Plot showing the frequency of traps containing multiple, one, or no QDs as a function of trap diameter. SEM images of (c) sub arrays of QDs, (d) a single QD in a trap before the PMMA liftoff step, (e) a single QD in a templated position after the PMMA liftoff step, and (f) multiple QDs in a templated position after the PMMA liftoff step. The contrast of the SEM images was adjusted after imaging to optimize visibility of particles and the array.

arrange single nano-diamonds and gold nanoparticles with diameters as small as 40 nm across millimeter-scale areas.[46,47] On a Si/SiO_2 substrate, electron beam lithography was used to define poly(methyl methacrylate) (PMMA) resist templates composed of 9 × 24 rectangular arrays of cylindrical traps with a 10 μm spacing and a depth of 157 nm, equal to the PMMA resist thickness. For every row, to optimize the capture of single 90 nm diameter silica-shelled QDs, the trap diameters were designed to increase from 90 to 170 nm in 10 nm increments, although the actual trap sizes were measured from SEM images to be larger (likely due to overexposure or overdeveloping) and to range from 122 to 238 nm in diameter (Section S7).

https://doi.org/10.1021/acsami.2c18475
ACS Appl. Mater. Interfaces 2023, 15, 4294−4302

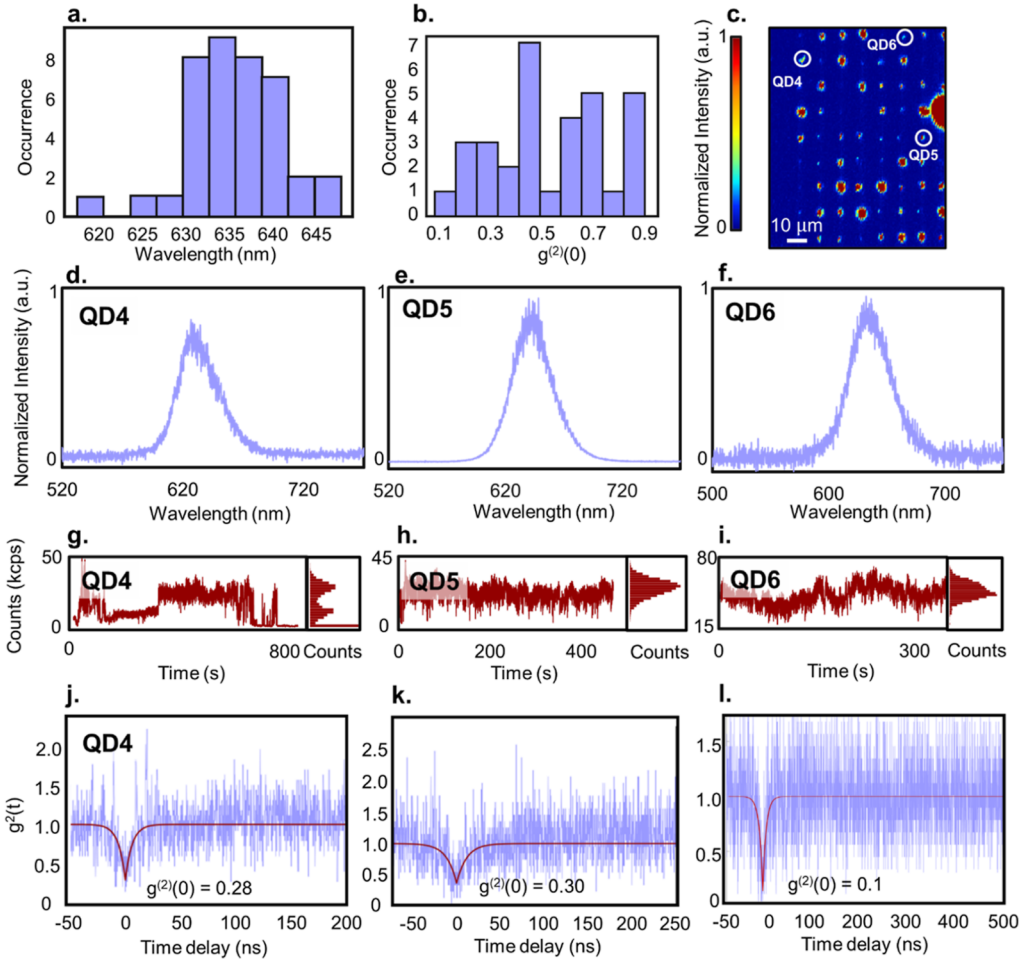

Figure 5. Quantum optical characterization of single silica-shelled QDs in a 9 × 24 array. (a) Distribution of emission maxima of 34 single silica-shelled QDs in array. (b) Distribution of outcomes from second-order autocorrelation function $g^{(2)}(\tau)$ of 32 single silica-shelled QDs. (c) PL image of single silica-coated QDs in a representative section of the templated array. (d–f) Single particle emission, (g–i) PL intensity time trace, and (j–l) second-order autocorrelation function $g^{(2)}(\tau)$ measurements of three representative single silica-shelled QDs in an array.

The assembly was performed in a home-built apparatus in which an aqueous dispersion of silica-coated QDs was deposited between a glass slide and the template surface. The QD dispersion was translated across the template surface at a speed of 2 μm/s by a motorized stage (Figure 3). A strong capillary force at the meniscus of the liquid rear edge drives the particles into the template traps.[28,32,33,46,69−71] During the assembly process, the environmental humidity (ambient dew point around −25 °C) and the substrate temperature (22 °C) were monitored and kept consistent as fluctuations of these factors can affect the assembly yield.[46] Finally, a liftoff step through immersion of the samples in *N*-methyl-2-pyrrolidone for 1 min and acetone for 1 min was done to remove the PMMA layer and any non-specifically bound QDs outside of the traps.

To obtain the yield for the QD assembly into the patterned array, SEM was used to image all 216 positions of one 9 × 24 array. Positioning of QDs in the entire array was tracked by taking images of subarrays to construct the large array image (Figure 4a). Full reconstruction of the array is shown in Section S10 of the Supporting Information. Ordered subarrays of QDs were clearly seen from the SEM images (Figure 4c), in which positions with a single QD (Figure 4d,e), multiple QDs (Figure 4f), and missing QDs could be clearly identified. Statistical characterization of the assembly showed that 75% of the traps were occupied by single QDs, 14% contained multiple QDs, and 11% were empty. Figure 4b shows that the optimal assembly yield for the silica-shelled QDs with an average diameter of 90 nm was achieved with a trap diameter of 160 nm, where only one position in the 24-member column was vacant. In addition, a smaller trap size (diameter < 150 nm) resulted in a higher frequency of missing QDs, and a larger trap size (diameter > 190 nm) exhibited a higher frequency of multiple QDs. From the SEM images of the array before the PMMA liftoff step (Figure 4d), we found that the single QDs tend to attach to the trap wall after assembling, indicating that the absolute position of single QDs from our technique is influenced heavily by the trap diameter. This leads to a trade-off between assembly yield and precise positioning, where larger traps result in better capturing of QDs, but less precision in the absolute position of the QDs.

2.4. Optical Characterization of Giant QDs in Arrays. Finally, we studied the optical properties of the giant QDs in the 9 × 24 array to compare with the ones on the planar substrate. It should be noted that measurements of QDs on the planar substrate and QDs in the array were taken 6 months apart. Figure 5a shows the distribution of emission maxima for 34 single QDs in the array. The majority of the emission peaks centered around 635 nm, consistent with the ensemble QD emission. To acquire the statistics for single-photon emission

https://doi.org/10.1021/acsami.2c18475
ACS Appl. Mater. Interfaces 2023, 15, 4294−4302

of the single giant QDs in the array, the second-order autocorrelation functions, $g^{(2)}(\tau)$, of 32 QDs were collected. Figure 5b displays the distribution of $g^{(2)}(0)$ values, where 16 QDs show photon antibunching behavior with $g^{(2)}(0) < 0.5$. The PL time traces of the measured QDs showed that emission bleaching occurred in less than 3.5 min for 11 QDs, between 3.5 and 10 min for 17 QDs, and after more than 10 min for 4 QDs. Additionally, blinking suppression was observed for 10 QDs. Figure 5c displays the PL map of a subarray highlighting three representative QD single-photon emitters with low $g^{(2)}(0)$ values. The optical characterization of these three QDs is shown in Figure 5d–l, where blinking suppression was seen in QD5 and QD6 and the $g^{(2)}(0)$ value was as low as 0.14 for QD6. Characterization of other QDs can be found in Sections S11 and S12 in Supporting Information. These results confirm that the silica-shelled QDs retained their the photostability and single-photon emission through the assembly process and over a long period of time, making them suitable for photonic device operation at room temperature. This is an important advance since colloidal materials often become unstable within weeks after their synthesis when left under ambient conditions.

3. CONCLUSIONS

A practical nanophotonics platform using colloidal materials as quantum emitters requires scalable integration. Our work presents a combination of a synthesis design to increase colloidal QD size through silica shelling with a template-assisted self-assembly technique to deterministically position giant QD single-photon emitters in a large array, which directly demonstrates the scalability advantage of colloidal materials for photonic devices. We have shown that template-assisted self-assembly allows placement of QD single-photon emitters into a large array with high assembly yield. The giant QDs both in the array and on planar substrates showed clear antibunching, characteristic of single-photon generation. It can be expected that optimization of the silica shelling process will maintain the superior PLQY of the starting CdSe/CdS and related core/shell QDs and may mitigate photobleaching issues, thus even further improving the single-photon emission properties of these materials. We envision that the demonstrated method of silica shelling may be applicable to other highly emissive nanomaterials such as halide perovskites or semiconductor QDs emitting in the IR range, which increases their stability and will advance the use of solution processable materials in the field of quantum nanophotonics. Finally, giant silica-shelled QDs are also a flexible class of materials that may be compatible with other device fabrication techniques to achieve deterministic single-particle positioning in complex photonic platforms.

4. EXPERIMENTAL SECTION

4.1. Materials. Syntheses of CdSe/CdS QDs were performed air-free. Silica shelling was done in ambient air in a well-ventilated fume hood or on a benchtop. All glassware was dried overnight in an oven at 160 °C. All chemicals listed below were used without further purification unless stated otherwise. Anhydrous ethanol (99.5%), anhydrous oleic acid (≥99%), anhydrous chloroform (99%), anhydrous toluene (99.5%), anhydrous methyl acetate (99.5%), 2-propanol (≥99.5%), acetone (≥99.5%), selenium powder (99.999%, 100 mesh), cadmium oxide powder (CdO, 99.9%), tri-noctylphosphine oxide (TOPO, 99%), trioctylphosphine (90%), 1-octanethiol (99%), octadence (ODE, 90%), tetraethyl orthosilicate (TEOS, 99.999%), Triton X-100, ammonium hydroxide solution (NH_4OH, 28.0–30.0% w/w), and *N*-methyl-2-pyrrolidone were purchased from MilliporeSigma and *n*-octadecylphosphonic acid (ODPA, 99%) was purchased from PCI Synthesis. Cadmium oleate was synthesized following a literature procedure.[52] 18.2 MΩ water was collected from an EMD Millipore purification system. UV–vis spectra were collected on a Cary 5000 spectrophotometer from Agilent. Steady-state PL measurements were taken on a HORIBA Jobin Yvon FluoroMax-4 fluorescence spectrophotometer and quantum yield measurements were taken with a Hamamatsu C9920-12 integrating sphere with a Hamamatsu C10027-01 photonic multi-channel analyzer.

4.2. Synthesis of CdSe/CdS QDs. Wurtzite core/shell CdSe/CdS QDs were synthesized using an established method with some minor modifications.[52] The synthesis of the CdSe core emitting at 620 nm was stopped 60 s after the injection of the Se-TOP solution. CdS shelling of the CdSe core was performed with 100 nanomole of CdSe QDs. The amounts of Cd- and S-precursors were calculated to achieve 9 monolayers of the CdS shells. To purify the QDs, ethyl acetate (15 mL) was mixed with the reaction solution and the QDs were precipitated by centrifugation at 7800 rpm for 6 min. The colorful precipitate was dissolved in hexane (7 mL) and the solution was centrifuged at 7800 rpm for 6 min to isolate unreacted precursors and byproducts from the QDs. The precipitate was discarded, and the red solution was mixed with ethyl acetate (15 mL), followed by another centrifugation at 7800 rpm for 6 min. The colorful precipitate was dissolved in chloroform (5 mL) and stored in a N_2-filled glovebox.

4.3. Silica Shelling of CdSe/CdS QDs. The CdSe/CdS QDs were shelled in silica spheres *via* the reverse microemulsion process.[57] To a mixture of 10 mL of cyclohexane, 1.9 mL of Triton X-100, 1.8 mL of hexanol, and 20 nmol of the CdSe/CdS QDs in chloroform were added. The mixture was stirred for 30 min, followed by dropwise addition of 200 μL of TEOS and stirring for another 15 min. Finally, 30 μL of ammonium hydroxide solution and 0.2 mL of water were injected successively. The reaction was stirred in the dark. After 3 days, a mixture (20 mL) of acetone and ethanol (1:1 ratio) was added to the solution followed by 5 min of centrifugation at 5000 rpm. The yellow precipitate was collected and washed with ethanol three times. The final product was dispersed in 5 mL of 18.2 MΩ water or ethanol and stored in air at room temperature.

4.4. Spin-Coating. To avoid aggregation of nanoparticles, a low concentration of the giant QD solution and a sonication step prior to fabrication were necessary. For the dynamic dispense spin-coating technique, 50 μL of the solution of giant QDs was dropped onto a substrate, which was rotating at 1500 rpm. The rotation was stopped after 30 s. For the static dispense spin-coating technique, 50 μL of the solution of giant QDs was dropped at the center of a silicon nitride chip. The rotation at 1500 rpm was started and then stopped after 30 s.

4.5. Template Fabrication and Assembly. Onto a single-side-polished Si wafer with a 280 nm thermal oxide layer, a PMMA positive resist (950 A4, Kayaku), was spun at 6000 rpm for 60 s followed by a soft bake at 180 °C for 120 s. Circular traps with design diameters ranging from 90 to 170 nm were created by electron beam lithography (Elionix ELS-7500EX) at a 50 kV accelerating voltage and a 50 pA beam current. The PMMA was developed in a 1:3 MIBK and isopropanol solution for 90 s. The substrate was cleaned by 6 s O_2 plasma treatment with 75 W and 20 sccm prior to assembly using a Gatan Solarus plasma cleaner. After the plasma treatment, the thickness of the PMMA layer was approximately 157 nm. The assembly was performed using a custom-built capillary assembly apparatus.[46] An aqueous dispersion of the silica-shelled QDs (about 5 μL) was deposited in between the patterned substrate and a glass slide. The substrate was translated by a motorized linear stage (New Focus Picomotor) at a speed of 2 μm/s. The whole process was performed in a home-built chamber equipped with a humidity-controlled setup. To maintain the temperature around 22 °C during the assembly process, the substrate was mounted on a water-cooled stage and monitored with a thermocouple. The ambient dew point was maintained around −25 °C. The liftoff of the PMMA template

https://doi.org/10.1021/acsami.2c18475
ACS Appl. Mater. Interfaces 2023, 15, 4294–4302

was done by immersing the assembled samples in *N*-methyl-2-pyrrolidone for 1 min, followed by 1 min in acetone.

4.6. Optical Setup. PL maps were obtained with a home-built confocal scanning PL setup. A 532 nm continuous-wave laser (Laserglow Technologies 532 nm DPSS Laser) was filtered through a 532 nm laser line filter and focused on the sample surface using a 100× (NA 0.95) objective lens to excite the QDs. A nano-positioning piezo stage (Physik Instrumente P-611.3S) was used to control the sample position. The QD PL was collected with the same objective and filtered through a 580 nm long pass filter and coupled into a fiber, which was either sent to an avalanche photodiode to create a PL map or to a spectrometer to obtain spectra of individual QDs. The spectral position and linewidth of the QD PL spectrum was then extracted by fitting the spectra to a Voigt line shape using a custom Python script and the SciPy software package. For $g^{(2)}(\tau)$ measurements, the signal was sent through a 1 × 2 fiber splitter with a 50/50 output ratio. Both output ends were connected to separate avalanche photodiodes (MPD-PDM). Their outputs were time correlated using a time tagger (PicoQuant TimeHarp 260). For all measurements, a custom software was used, which mapped a specific area of the sample first and allowed us to select specific spots. At the same time, the PL counts at that site were displayed live during the measurement. For QDs in arrays, all potential sites of the array were probed and if the single emitter/ensemble did not bleach, then spectra, $g^{(2)}(t)$, and PL were collected. For samples, where QDs were spin-coated, we considered emitters that appeared as isolated spots in the PL map and showed a PL count larger than 3k and less than 50k.

■ ASSOCIATED CONTENT

Supporting Information

The Supporting Information is available free of charge at https://pubs.acs.org/doi/10.1021/acsami.2c18475.

Additional details of QD synthesis and characterization; additional TEM and SEM images; and additional single-particle measurements (PDF)

■ AUTHOR INFORMATION

Corresponding Author

Brandi M. Cossairt − *Department of Chemistry, University of Washington, Seattle, Washington 98189, United States;* orcid.org/0000-0002-9891-3259; Email: cossairt@uw.edu

Authors

Hao A. Nguyen − *Department of Chemistry, University of Washington, Seattle, Washington 98189, United States;* orcid.org/0000-0001-6742-1748

David Sharp − *Department of Physics, University of Washington, Seattle, Washington 98185, United States;* orcid.org/0000-0002-1034-8567

Johannes E. Fröch − *Department of Physics, University of Washington, Seattle, Washington 98185, United States; Department of Electrical and Computer Engineering, University of Washington, Seattle, Washington 98195, United States*

Yi-Yu Cai − *Department of Electrical and Systems Engineering, University of Pennsylvania, Philadelphia, Pennsylvania 19104, United States*

Shenwei Wu − *Department of Chemistry, University of Washington, Seattle, Washington 98189, United States*

Madison Monahan − *Department of Chemistry, University of Washington, Seattle, Washington 98189, United States*

Christopher Munley − *Department of Physics, University of Washington, Seattle, Washington 98185, United States*

Arnab Manna − *Department of Physics, University of Washington, Seattle, Washington 98185, United States*

Arka Majumdar − *Department of Physics, University of Washington, Seattle, Washington 98185, United States; Department of Electrical and Computer Engineering, University of Washington, Seattle, Washington 98195, United States;* orcid.org/0000-0003-0917-590X

Cherie R. Kagan − *Department of Electrical and Systems Engineering, University of Pennsylvania, Philadelphia, Pennsylvania 19104, United States; Department of Materials Science and Engineering and Department of Chemistry, University of Pennsylvania, Philadelphia, Pennsylvania 19104, United States;* orcid.org/0000-0001-6540-2009

Complete contact information is available at: https://pubs.acs.org/10.1021/acsami.2c18475

Notes

The authors declare no competing financial interest.

■ ACKNOWLEDGMENTS

This material was based upon work supported by the National Science Foundation. Grant no. DMR-2019444 supported the template-directed assembly of silica-coated QDs, all single-particle measurements, and characterization of the positioned QDs. Grant no. OMA-1936100 supported the synthesis of silica-coated QDs and material characterization. Part of this work was carried out at the Singh Center for Nanotechnology, which was supported by the NSF National Nanotechnology Coordinated Infrastructure Program under grant NNCI-2025608. Part of this work was conducted at the Molecular Analysis Facility, a National Nanotechnology Coordinated Infrastructure site at the University of Washington, which was supported in part by funds from the National Science Foundation (awards NNCI-2025489 and NNCI-1542101), the Molecular Engineering & Sciences Institute, and the Clean Energy Institute.

■ REFERENCES

(1) Madsen, L. S.; Laudenbach, F.; Askarani, M. F..; Rortais, F.; Vincent, T.; Bulmer, J. F. F.; Miatto, F. M.; Neuhaus, L.; Helt, L. G.; Collins, M. J.; Lita, A. E.; Gerrits, T.; Nam, S. W.; Vaidya, V. D.; Menotti, M.; Dhand, I.; Vernon, Z.; Quesada, N.; Lavoie, J. Quantum Computational Advantage with a Programmable Photonic Processor. *Nature* **2022**, *606*, 75−81.

(2) Wang, H.; Qin, J.; Ding, X.; Chen, M.-C.; Chen, S.; You, X.; He, Y.-M.; Jiang, X.; You, L.; Wang, Z.; Schneider, C.; Renema, J. J.; Höfling, S.; Lu, C.-Y.; Pan, J.-W. Boson Sampling with 20 Input Photons and a 60-Mode Interferometer in a1014-Dimensional Hilbert Space. *Phys. Rev. Lett.* **2019**, *123*, 250503.

(3) Majumdar, A.; Rundquist, A.; Bajcsy, M.; Dasika, V. D.; Bank, S. R.; Vučković, J. Design and Analysis of Photonic Crystal Coupled Cavity Arrays for Quantum Simulation. *Phys. Rev. B: Condens. Matter Mater. Phys.* **2012**, *86*, 195312.

(4) Warburton, R. J. Single Spins in Self-Assembled Quantum Dots. *Nat. Mater.* **2013**, *12*, 483−493.

(5) Buckley, S.; Rivoire, K.; Vučković, J. Engineered Quantum Dot Single-Photon Sources. *Rep. Prog. Phys.* **2012**, *75*, 126503.

(6) Sajid, A.; Ford, M. J.; Reimers, J. R. Single-Photon Emitters in Hexagonal Boron Nitride: A Review of Progress. *Rep. Prog. Phys.* **2020**, *83*, 044501.

(7) Nikolay, N.; Mendelson, N.; Özelci, E.; Sontheimer, B.; Böhm, F.; Kewes, G.; Toth, M.; Aharonovich, I.; Benson, O. Direct Measurement of Quantum Efficiency of Single-Photon Emitters in Hexagonal Boron Nitride. *Optica* **2019**, *6*, 1084−1088.

(8) Fröch, J. E.; Kim, S.; Mendelson, N.; Kianinia, M.; Toth, M.; Aharonovich, I. Coupling Hexagonal Boron Nitride Quantum Emitters to Photonic Crystal Cavities. *ACS Nano* **2020**, *14*, 7085−7091.
(9) Dolan, P. R.; Adekanye, S.; Trichet, A. A. P.; Johnson, S.; Flatten, L. C.; Chen, Y. C.; Weng, L.; Hunger, D.; Chang, H.-C.; Castelletto, S.; Smith, J. M. Robust, Tunable, and High Purity Triggered Single Photon Source at Room Temperature Using a Nitrogen-Vacancy Defect in Diamond in an Open Microcavity. *Opt. Express* **2018**, *26*, 7056−7065.
(10) Bradac, C.; Gao, W.; Forneris, J.; Trusheim, M. E.; Aharonovich, I. Quantum Nanophotonics with Group IV Defects in Diamond. *Nat. Commun.* **2019**, *10*, 5625.
(11) Ren, S.; Tan, Q.; Zhang, J. Review on the Quantum Emitters in Two-Dimensional Materials. *J. Semiconduct.* **2019**, *40*, 071903.
(12) Zhou, X.; Zhang, Z.; Guo, W. Dislocations as Single Photon Sources in Two-Dimensional Semiconductors. *Nano Lett.* **2020**, *20*, 4136−4143.
(13) Saha, U.; Siverns, J. D.; Hannegan, J.; Prabhu, M.; Bersin, E.; Bandyopadhyay, S.; Carolan, J.; Quraishi, Q.; Englund, D.; Waks, E. Routing Single Photons from a Trapped Ion with Photonic Integrated Circuits. In *Conference on Lasers and Electro-Optics*; Technical Digest Series; Optica Publishing Group: San Jose, California, 2022. FTh5O.1.
(14) Higginbottom, D. B.; Slodička, L.; Araneda, G.; Lachman, L.; Filip, R.; Hennrich, M.; Blatt, R. Pure Single Photons from a Trapped Atom Source. *New J. Phys.* **2016**, *18*, 093038.
(15) Toninelli, C.; Gerhardt, I.; Clark, A. S.; Reserbat-Plantey, A.; Götzinger, S.; Ristanović, Z.; Colautti, M.; Lombardi, P.; Major, K. D.; Deperasińska, I.; Pernice, W. H.; Koppens, F. H. L.; Kozankiewicz, B.; Gourdon, A.; Sandoghdar, V.; Orrit, M. Single Organic Molecules for Photonic Quantum Technologies. *Nat. Mater.* **2021**, *20*, 1615−1628.
(16) Lombardi, P.; Trapuzzano, M.; Colautti, M.; Margheri, G.; Degiovanni, I. P.; López, M.; Kück, S.; Toninelli, C. A Molecule-Based Single-Photon Source Applied in Quantum Radiometry. *Adv. Quantum Technol.* **2020**, *3*, 1900083.
(17) Aharonovich, I.; Englund, D.; Toth, M. Solid-State Single-Photon Emitters. *Nat. Photonics* **2016**, *10*, 631−641.
(18) Kagan, C. R.; Bassett, L. C.; Murray, C. B.; Thompson, S. M. Colloidal Quantum Dots as Platforms for Quantum Information Science. *Chem. Rev.* **2021**, *121*, 3186−3233.
(19) Chen, Y.; Sharp, D.; Saxena, A.; Nguyen, H.; Cossairt, B. M.; Majumdar, A. Integrated Quantum Nanophotonics with Solution-Processed Materials. *Adv. Quantum Technol.* **2022**, *5*, 2100078.
(20) Zhu, C.; Marczak, M.; Feld, L.; Boehme, S. C.; Bernasconi, C.; Moskalenko, A.; Cherniukh, I.; Dirin, D.; Bodnarchuk, M. I.; Kovalenko, M. V.; Rainò, G. Room-Temperature, Highly Pure Single-Photon Sources from All-Inorganic Lead Halide Perovskite Quantum Dots. *Nano Lett.* **2022**, *22*, 3751−3760.
(21) Michler, P.; Imamoğlu, A.; Mason, M. D.; Carson, P. J.; Strouse, G. F.; Buratto, S. K. Quantum Correlation among Photons from a Single Quantum Dot at Room Temperature. *Nature* **2000**, *406*, 968−970.
(22) Chandrasekaran, V.; Tessier, M. D.; Dupont, D.; Geiregat, P.; Hens, Z.; Brainis, E. Nearly Blinking-Free, High-Purity Single-Photon Emission by Colloidal InP/ZnSe Quantum Dots. *Nano Lett.* **2017**, *17*, 6104−6109.
(23) Sebald, K.; Michler, P.; Passow, T.; Hommel, D.; Bacher, G.; Forchel, A. Single-Photon Emission of CdSe Quantum Dots at Temperatures up to 200 K. *Appl. Phys. Lett.* **2002**, *81*, 2920−2922.
(24) Lin, X.; Dai, X.; Pu, C.; Deng, Y.; Niu, Y.; Tong, L.; Fang, W.; Jin, Y.; Peng, X. Electrically-Driven Single-Photon Sources Based on Colloidal Quantum Dots with near-Optimal Antibunching at Room Temperature. *Nat. Commun.* **2017**, *8*, 1132.
(25) Morozov, S.; Pensa, E. L.; Khan, A. H.; Polovitsyn, A.; Cortés, E.; Maier, S. A.; Vezzoli, S.; Moreels, I.; Sapienza, R. Electrical Control of Single-Photon Emission in Highly Charged Individual Colloidal Quantum Dots. *Sci. Adv.* **2020**, *6*, No. eabb1821.
(26) Chen, Y.; Ryou, A.; Friedfeld, M. R.; Fryett, T.; Whitehead, J.; Cossairt, B. M.; Majumdar, A. Deterministic Positioning of Colloidal Quantum Dots on Silicon Nitride Nanobeam Cavities. *Nano Lett.* **2018**, *18*, 6404−6410.
(27) Xu, X.; Jin, S. Strong Coupling of Single Quantum Dots with Low-Refractive-Index/High-Refractive-Index Materials at Room Temperature. *Sci. Adv.* **2020**, *6*, No. eabb3095.
(28) Cui, Y.; Björk, M. T.; Liddle, J. A.; Sönnichsen, C.; Boussert, B.; Alivisatos, A. P. Integration of Colloidal Nanocrystals into Lithographically Patterned Devices. *Nano Lett.* **2004**, *4*, 1093−1098.
(29) Yadav, R. K.; Liu, W.; Li, R.; Odom, T. W.; Agarwal, G. S.; Basu, J. K. Room-Temperature Coupling of Single Photon Emitting Quantum Dots to Localized and Delocalized Modes in a Plasmonic Nanocavity Array. *ACS Photonics* **2021**, *8*, 576−584.
(30) Yadav, R. K.; Bourgeois, M. R.; Cherqui, C.; Juarez, X. G.; Wang, W.; Odom, T. W.; Schatz, G. C.; Basu, J. K. Room Temperature Weak-to-Strong Coupling and the Emergence of Collective Emission from Quantum Dots Coupled to Plasmonic Arrays. *ACS Nano* **2020**, *14*, 7347−7357.
(31) Brokmann, X.; Messin, G.; Desbiolles, P.; Giacobino, E.; Dahan, M.; Hermier, J. P. Colloidal CdSe/ZnS Quantum Dots as Single-Photon Sources. *New J. Phys.* **2004**, *6*, 99.
(32) Holzner, F.; Kuemin, C.; Paul, P.; Hedrick, J. L.; Wolf, H.; Spencer, N. D.; Duerig, U.; Knoll, A. W. Directed Placement of Gold Nanorods Using a Removable Template for Guided Assembly. *Nano Lett.* **2011**, *11*, 3957−3962.
(33) Malaquin, L.; Kraus, T.; Schmid, H.; Delamarche, E.; Wolf, H. Controlled Particle Placement through Convective and Capillary Assembly. *Langmuir* **2007**, *23*, 11513−11521.
(34) Eich, A.; Spiekermann, T. C.; Gehring, H.; Sommer, L.; Bankwitz, J. R.; Schrinner, P. P. J.; Preuß, J. A.; Michaelis de Vasconcellos, S.; Bratschitsch, R.; Pernice, W. H. P.; Schuck, C. Single-Photon Emission from Individual Nanophotonic-Integrated Colloidal Quantum Dots. *ACS Photonics* **2022**, *9*, 551−558.
(35) Zhang, Q.; Dang, C.; Urabe, H.; Wang, J.; Sun, S.; Nurmikko, A. Large Ordered Arrays of Single Photon Sources Based on II−VI Semiconductor Colloidal Quantum Dot. *Opt. Express* **2008**, *16*, 19592−19599.
(36) Kim, J.-H.; Aghaeimeibodi, S.; Richardson, C. J. K.; Leavitt, R. P.; Englund, D.; Waks, E. Hybrid Integration of Solid-State Quantum Emitters on a Silicon Photonic Chip. *Nano Lett.* **2017**, *17*, 7394−7400.
(37) Davanco, M.; Liu, J.; Sapienza, L.; Zhang, C.-Z.; De Miranda Cardoso, J. V.; Verma, V.; Mirin, R.; Nam, S. W.; Liu, L.; Srinivasan, K. Heterogeneous Integration for On-Chip Quantum Photonic Circuits with Single Quantum Dot Devices. *Nat. Commun.* **2017**, *8*, 889.
(38) Kolchin, P.; Pholchai, N.; Mikkelsen, M. H.; Oh, J.; Ota, S.; Islam, M. S.; Yin, X.; Zhang, X. High Purcell Factor Due To Coupling of a Single Emitter to a Dielectric Slot Waveguide. *Nano Lett.* **2015**, *15*, 464−468.
(39) Cohen, T. A.; Sharp, D.; Kluherz, K. T.; Chen, Y.; Munley, C.; Anderson, R. T.; Swanson, C. J.; De Yoreo, J. J.; Luscombe, C. K.; Majumdar, A.; Gamelin, D. R.; Mackenzie, J. D. Direct Patterning of Perovskite Nanocrystals on Nanophotonic Cavities with Electrohydrodynamic Inkjet Printing. *Nano Lett.* **2022**, *22*, 5681−5688.
(40) Nann, T.; Mulvaney, P. Single Quantum Dots in Spherical Silica Particles. *Angew. Chem., Int. Ed.* **2004**, *43*, 5393−5396.
(41) Ma, Y.; Li, Y.; Ma, S.; Zhong, X. Highly Bright Water-Soluble Silica Coated Quantum Dots with Excellent Stability. *J. Mater. Chem. B* **2014**, *2*, 5043−5051.
(42) Hu, X.; Zrazhevskiy, P.; Gao, X. Encapsulation of Single Quantum Dots with Mesoporous Silica. *Ann. Biomed. Eng.* **2009**, *37*, 1960−1966.
(43) Goftman, V. V.; Aubert, T.; Ginste, D. V.; Van Deun, R.; Beloglazova, N. V.; Hens, Z.; De Saeger, S.; Goryacheva, I. Y. Synthesis, modification, bioconjugation of silica coated fluorescent quantum dots and their application for mycotoxin detection. *Biosens. Bioelectron.* **2016**, *79*, 476−481.

https://doi.org/10.1021/acsami.2c18475
ACS Appl. Mater. Interfaces 2023, 15, 4294−4302

(44) Aubert, T.; Soenen, S. J.; Wassmuth, D.; Cirillo, M.; Van Deun, R.; Braeckmans, K.; Hens, Z. Bright and Stable CdSe/CdS@SiO2 Nanoparticles Suitable for Long-Term Cell Labeling. *ACS Appl. Mater. Interfaces* **2014**, *6*, 11714−11723.
(45) Huang, Y.; Cohen, T. A.; Sperry, B. M.; Larson, H.; Nguyen, H. A.; Homer, M. K.; Dou, F. Y.; Jacoby, L. M.; Cossairt, B. M.; Gamelin, D. R.; Luscombe, C. K. Organic Building Blocks at Inorganic Nanomaterial Interfaces. *Mater. Horiz.* **2022**, *9*, 61−87.
(46) Shulevitz, H. J.; Huang, T.-Y.; Xu, J.; Neuhaus, S. J.; Patel, R. N.; Choi, Y. C.; Bassett, L. C.; Kagan, C. R. Template-Assisted Self-Assembly of Fluorescent Nanodiamonds for Scalable Quantum Technologies. *ACS Nano* **2022**, *16*, 1847−1856.
(47) Greybush, N. J.; Pacheco-Peña, V.; Engheta, N.; Murray, C. B.; Kagan, C. R. Plasmonic Optical and Chiroptical Response of Self-Assembled Au Nanorod Equilateral Trimers. *ACS Nano* **2019**, *13*, 1617−1624.
(48) Chen, Y.; Vela, J.; Htoon, H.; Casson, J. L.; Werder, D. J.; Bussian, D. A.; Klimov, V. I.; Hollingsworth, J. A. "Giant" Multishell CdSe Nanocrystal Quantum Dots with Suppressed Blinking. *J. Am. Chem. Soc.* **2008**, *130*, 5026−5027.
(49) Gong, K.; Kelley, D. F. Lattice Strain Limit for Uniform Shell Deposition in Zincblende CdSe/CdS Quantum Dots. *J. Phys. Chem. Lett.* **2015**, *6*, 1559−1562.
(50) Pahomi, T. E.; Cheche, T. O. Strain Influence on Optical Absorption of Giant Semiconductor Colloidal Quantum Dots. *Chem. Phys. Lett.* **2014**, *612*, 33−38.
(51) Rafipoor, M.; Dupont, D.; Tornatzky, H.; Tessier, M. D.; Maultzsch, J.; Hens, Z.; Lange, H. Strain Engineering in InP/(Zn,Cd)Se Core/Shell Quantum Dots. *Chem. Mater.* **2018**, *30*, 4393−4400.
(52) Hanifi, D. A.; Bronstein, N. D.; Koscher, B. A.; Nett, Z.; Swabeck, J. K.; Takano, K.; Schwartzberg, A. M.; Maserati, L.; Vandewal, K.; van de Burgt, Y.; Salleo, A.; Alivisatos, A. P. Redefining Near-Unity Luminescence in Quantum Dots with Photothermal Threshold Quantum Yield. *Science* **2019**, *363*, 1199−1202.
(53) Chen, O.; Zhao, J.; Chauhan, V. P.; Cui, J.; Wong, C.; Harris, D. K.; Wei, H.; Han, H.-S.; Fukumura, D.; Jain, R. K.; Bawendi, M. G. Compact High-Quality CdSe−CdS Core−Shell Nanocrystals with Narrow Emission Linewidths and Suppressed Blinking. *Nat. Mater.* **2013**, *12*, 445−451.
(54) Darbandi, M.; Thomann, R.; Nann, T. Single Quantum Dots in Silica Spheres by Microemulsion Synthesis. *Chem. Mater.* **2005**, *17*, 5720−5725.
(55) Yang, Y.; Jing, L.; Yu, X.; Yan, D.; Gao, M. Coating Aqueous Quantum Dots with Silica via Reverse Microemulsion Method: Toward Size-Controllable and Robust Fluorescent Nanoparticles. *Chem. Mater.* **2007**, *19*, 4123−4128.
(56) Selvan, S. T.; Tan, T. T.; Ying, J. Y. Robust, Non-Cytotoxic, Silica-Coated CdSe Quantum Dots with Efficient Photoluminescence. *Adv. Mater.* **2005**, *17*, 1620−1625.
(57) Wang, N.; Koh, S.; Jeong, B. G.; Lee, D.; Kim, W. D.; Park, K.; Nam, M. K.; Lee, K.; Kim, Y.; Lee, B.-H.; Lee, K.; Bae, W. K.; Lee, D. C. Highly Luminescent Silica-Coated CdS/CdSe/CdS Nanoparticles with Strong Chemical Robustness and Excellent Thermal Stability. *Nanotechnology* **2017**, *28*, 185603.
(58) Zhang, A.; Chen, L.; Wang, M.; Li, J.; Chen, L.; Shi, R.; Zhang, N.; Yang, P. Study on the Luminescence Stability of CdSe/CdxZn1-XS Quantum Dots during the Silication Process. *J. Lumin.* **2020**, *219*, 116907.
(59) Anderson, B. D.; Wu, W.-C.; Tracy, J. B. Silica Overcoating of CdSe/CdS Core/Shell Quantum Dot Nanorods with Controlled Morphologies. *Chem. Mater.* **2016**, *28*, 4945−4952.
(60) Wang, X.; Li, W.; Zhao, B.; Zhang, D.; Sun, K.; An, X.; Zhang, Z.; Shen, Z. Highly Fluorescent Quantum Dot@silica Nanoparticles by a Novel Post-Treatment for Live Cell Imaging. *RSC Adv.* **2013**, *3*, 3553−3556.
(61) Goryacheva, O. A.; Wegner, K. D.; Sobolev, A. M.; Häusler, I.; Gaponik, N.; Goryacheva, I. Y.; Resch-Genger, U. Influence of Particle Architecture on the Photoluminescence Properties of Silica-Coated CdSe Core/Shell Quantum Dots. *Anal. Bioanal. Chem.* **2022**, *414*, 4427−4439.
(62) Cao, H.; Ma, J.; Huang, L.; Qin, H.; Meng, R.; Li, Y.; Peng, X. Design and Synthesis of Antiblinking and Antibleaching Quantum Dots in Multiple Colors via Wave Function Confinement. *J. Am. Chem. Soc.* **2016**, *138*, 15727−15735.
(63) Qin, H.; Meng, R.; Wang, N.; Peng, X. Photoluminescence Intermittency and Photo-Bleaching of Single Colloidal Quantum Dot. *Adv. Mater.* **2017**, *29*, 1606923.
(64) van Sark, W. G. J. H. M.; Frederix, P. L. T. M.; Bol, A. A.; Gerritsen, H. C.; Meijerink, A. Blueing, Bleaching, and Blinking of Single CdSe/ZnS Quantum Dots. *ChemPhysChem* **2002**, *3*, 871−879.
(65) Lee, S. F.; Osborne, M. A. Brightening, Blinking, Bluing and Bleaching in the Life of a Quantum Dot: Friend or Foe? *ChemPhysChem* **2009**, *10*, 2174−2191.
(66) Orfield, N. J.; McBride, J. R.; Wang, F.; Buck, M. R.; Keene, J. D.; Reid, K. R.; Htoon, H.; Hollingsworth, J. A.; Rosenthal, S. J. Quantum Yield Heterogeneity among Single Nonblinking Quantum Dots Revealed by Atomic Structure-Quantum Optics Correlation. *ACS Nano* **2016**, *10*, 1960−1968.
(67) Yuan, Z.; Kardynal, B. E.; Stevenson, R. M.; Shields, A. J.; Lobo, C. J.; Cooper, K.; Beattie, N. S.; Ritchie, D. A.; Pepper, M. Electrically Driven Single-Photon Source. *Science* **2002**, *295*, 102−105.
(68) Brokmann, X.; Giacobino, E.; Dahan, M.; Hermier, J. P. Highly Efficient Triggered Emission of Single Photons by Colloidal CdSe/ZnS Nanocrystals. *Appl. Phys. Lett.* **2004**, *85*, 712−714.
(69) Yin, Y.; Lu, Y.; Gates, B.; Xia, Y. Template-Assisted Self-Assembly: A Practical Route to Complex Aggregates of Monodispersed Colloids with Well-Defined Sizes, Shapes, and Structures. *J. Am. Chem. Soc.* **2001**, *123*, 8718−8729.
(70) Mehraeen, S.; Asbahi, M.; Fuke, W.; Yang, J. K. W.; Cao, J.; Tan, M. C. Directed Self-Assembly of Sub-10 Nm Particles: Role of Driving Forces and Template Geometry in Packing and Ordering. *Langmuir* **2015**, *31*, 8548−8557.
(71) Asbahi, M.; Mehraeen, S.; Wang, F.; Yakovlev, N.; Chong, K. S. L.; Cao, J.; Tan, M. C.; Yang, J. K. W. Large Area Directed Self-Assembly of Sub-10 Nm Particles with Single Particle Positioning Resolution. *Nano Lett.* **2015**, *15*, 6066−6070.

https://doi.org/10.1021/acsami.2c18475
ACS Appl. Mater. Interfaces 2023, 15, 4294−4302